

Two-Dimensional Numerical Simulations of a Solid State Maxwell Demon

Andrew R. Putnam

*Departments of Physics and Electrical Engineering
University of San Diego, San Diego, CA 92110
aputnam@sandiego.edu*

Abstract: Numerical simulations of the solid-state Maxwell demon proposed by Sheehan, Putnam, and Wright (2002) are presented. These verify the results of the original 1-D analytical model. A detailed description of the 2-D device simulator is given.

INTRODUCTION

Recently, a novel solid-state challenge to the second law has been proposed by Sheehan, Putnam, and Wright (2002) [1]. 1-D analytical calculations indicate that, under realistic physical conditions, the device should be able to generate power densities on the order of 10^8 W/m³ or greater. A more detailed explanation of this can be found in this volume [2].

Two dimensional numerical simulations of this device were performed to check the general conclusions of Sheehan's one-dimensional model. The simulations were performed using Silvaco International's ATLAS 2-D semiconductor device simulator software with S-Pisces and Giga modules. These simulations were performed over a wide variation of experimental parameters. The 2-D model shows good agreement with the primary findings of the 1-D model.

The extraordinary cost and effort required to produce semiconductor prototypes prohibits creating the device without support from a major semiconductor manufacturer. Even major semiconductor manufacturers, as well as researchers, instead use semiconductor device simulation software to model the characteristics of the device at a fraction of the cost and effort.

Ideally, these simulators would be able to solve any equations relevant to any semiconductor device using a full three-dimensional model. Unfortunately, the complexity of this kind of simulation would make the processing time to run the simulation far too long. Instead, the simulators make some approximations and only use the models they deem relevant to a given device. In this way, the simulators retain much of their accuracy while reducing simulation times to more reasonable levels.

ATLAS SEMICONDUCTOR SIMULATOR

Silvaco International Corporation's ATLAS [3] is a semiconductor simulator that has been used extensively in academia and industry. Notable companies that use ATLAS are Advanced Micro Devices Corporation, Harris Semiconductor, NASA, Sensitron Semiconductor, and Science Applications International Corporation (SAIC). Academic institutions that use ATLAS include the University of California at Berkeley, Stanford University, and the University of California at San Diego. ATLAS has been continually refined since the 1970's to be more realistic for a wide range of semiconductor device configurations.

The S-Pisces module of ATLAS focuses on accurate device simulation for silicon devices. Important features of the S-Pisces module include: drift-diffusion and energy balance transport equations, surface/bulk mobility, incomplete ionization, bandgap narrowing, Shockley-Reed-Hall and Auger recombination, impact ionization, band-to-band and Fowler-Nordheim tunneling models, and trap and defect modeling. The underlying model for S-Pisces simulations is the Shockley-Reed-Hall model, but additional models can be used by the device simulator if the simulator deems the models to be applicable or if the user explicitly directs the simulator to use additional models.

The Giga module allows S-Pisces to correct for non-isothermal properties of the device, including: heat generation, heat flow, lattice heating, heat sinks, and the effect of local temperature on physical constants. Since the *standard device* is modeled under room temperature conditions, the isothermal effects accounted for by Giga should be limited to local thermal fluctuations. The Giga model does allow simulations at temperatures far below and far above a typical terrestrial environment, but all of the simulations were performed at room temperature ($T = 300$ K).

ATLAS solves three fundamental types of equations when simulating a semiconductor device: Poisson's equation, the continuity equations, and the transport equations, including the drift-diffusion transport model, energy balance transport model, and the hydrodynamic model. Poisson's equation relates the space charge density to electrostatic potential, and allows calculation of electric fields based on the potential. The transport equations are all derivative of the Boltzmann transport equation. For most applications, the drift-diffusion transport model is used. Only for extremely small, deep submicron devices are the energy balance transport or hydrodynamic models deemed necessary for the simulation.

Unfortunately, neither ATLAS nor any other commercially available semiconductor simulator is capable of solving full time-dependant equations, so here every solution is an equilibrium solution. The time scales associated with the motion of the device must therefore be addressed to determine if a collection of equilibrium solutions accurately models the time-dependant behavior of the device.

SIMULATIONS

The majority of the simulations performed followed the same dimensions as the device discussed by Sheehan, Putnam, and Wright [1], referred to as the *standard device*.

The device is shown in Figure 1. It is essentially two horseshoe-shaped pieces of n- and p-doped semiconductor facing each other. At one adjoining region, referred to as Junction I (J-I), the two pieces are physically joined. At the other region, referred to as Junction II (J-II), the pieces are separated by a small vacuum gap of width X_g . The overall length and width of the device, X_{dev} , are equal. The typical relevant parameters of the *standard device* are: $X_{dev} = 10^{-6}$ m, $X_g = 3 \times 10^{-8}$ m, $N_A = N_D = 10^{21}$ m⁻³. Simulations using a wide variation in these parameters ($10^{17} = N_{A,D} = 10^{26}$ m⁻³, $10^{-8} = X_g = 3 \times 10^{-7}$ m) were also performed. The device is composed of silicon doped with generic donors/acceptors, and surrounded by vacuum. The generic dopants allow ATLAS to run the simulations without considering the lattice deformation and defects caused by real dopants.

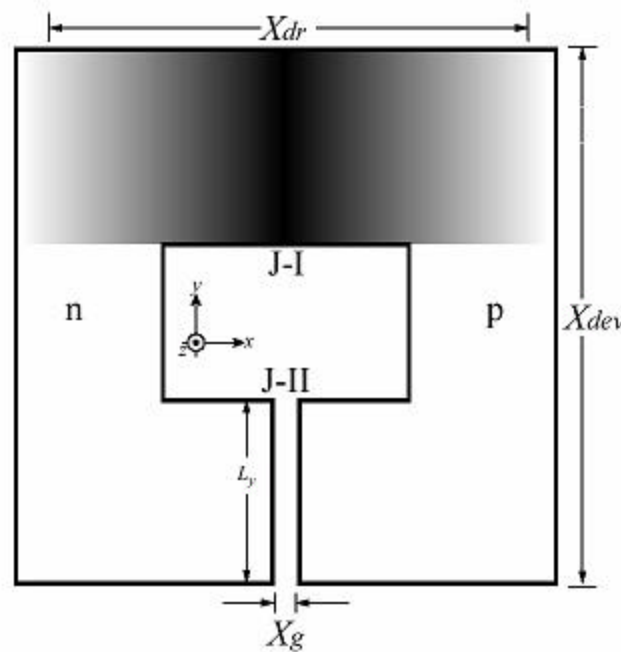


FIGURE 1 – *Standard device* with junctions I and II, physical dimensions, and standard coordinates indicated. The shaded region in Junction I represents the depletion region.

The doping concentration is small enough so that the device should not be subject to heavy doping effects, such as bandgap narrowing and incomplete ionization of impurities. ATLAS does not account for heavy doping effects until doping levels above 10^{24} m⁻³. At 10^{21} m⁻³, the *standard device* is well below the threshold at which heavy doping effects should affect the simulations. As such, the Boltzmann carrier statistics model is used rather than Fermi-Dirac carrier statistics, and the simulator is not directed to account for heavy doping effects.

To check the validity of the 1-D analytical model, numerous simulations were run varying the primary physical parameters of the system: gap width (X_g), device scale size (X_{dev}), and dopant concentration (N_A , N_D). These verified the primary results of the 1-D analytical model. For example, Figure 2 shows the simulation results for the mid-channel

electric field in the gap region, and compares those results to the predicted electric field strength in the 1-D analytical model as gap width is varied. The two models show good agreement, within a factor of 2 or less, for gap sizes greater than 5×10^{-8} m. At smaller gap widths, the two models begin to diverge, but show the same general trend of electric field changing inversely with gap width. The difference between the two models is due to the unphysical singularity in the 1-D model at a gap width $X_g = 0$. The simulations are not subject to this singularity; instead, the larger electric fields disperse the charge carriers, thus moderating the electric field strength. The approximate saturation point for the electric field in the gap for the simulations is 10^7 V/m, well below the dielectric strength of silicon.

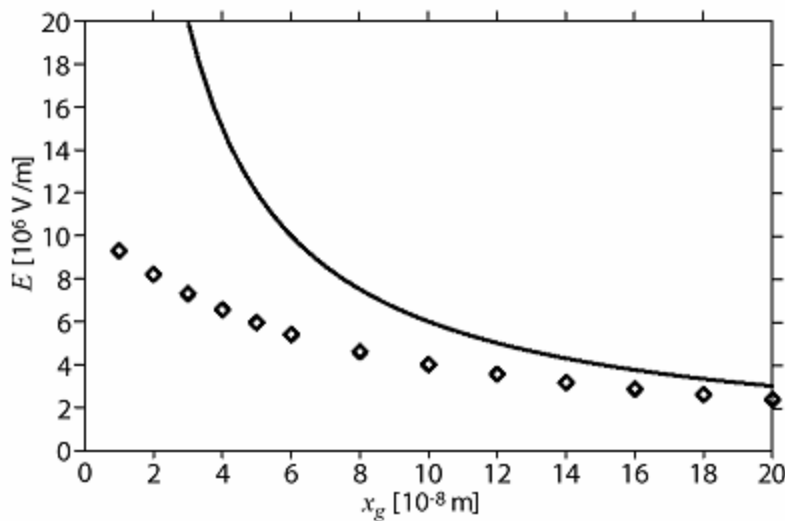


FIGURE 2 – Electric field strength versus gap width in the J-II region of the *standard device* for 1-D analytical model (solid line) and 2-D ATLAS simulations (open diamonds).

The electrostatic potential energy versus gap width for the 1-D model and the 2-D simulations are shown in Figure 3. The potential energy is calculated from $E_{es} = \frac{\epsilon_0 E^2}{2}$ for vacuum and $E_{es} = \frac{\mathbf{k}\epsilon_0 E^2}{2}$ for silicon, integrated over their respective regions. The energy of the 1-D model is normalized in the z-direction so that it conforms to the output from the 2-D simulations. Once again, the two models show good agreement at larger gap widths, but diverge as the gap narrows. This is also a consequence of the unphysical discontinuity at $X_g = 0$ for the 1-D analytical model. The models agree within a factor of 2 for gap widths of 2×10^{-8} m and higher, so despite the inherent shortcomings of the 1-D model, the results for electrostatic energy that the 1-D model gives are surprisingly close to the more realistic and complex 2-D simulation results.

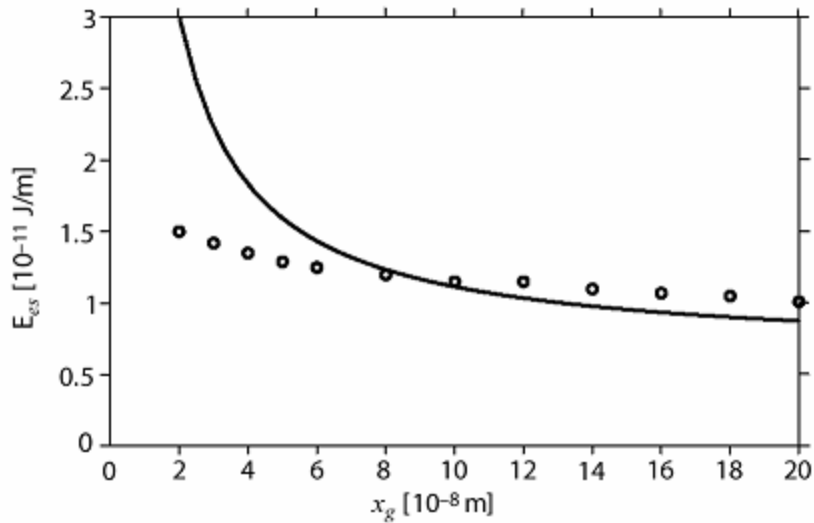


FIGURE 3 – Electrostatic potential energy versus gap width in the J-II region of the *standard device* for 1-D analytical model (solid line) and 2-D ATLAS simulations (open circles). The energy for the 1-D model is normalized with respect to the z -direction to conform to the output of the 2-D model.

Simulations were then run to investigate the linear electrostatic motor, shown in Figure 4. A rectangular slab of intrinsically doped semiconductor ($l_x=300\text{?}$, $l_y=600\text{?}$) called the piston is inserted into the J-II gap at different locations. A series of 17 simulations were run over equal distance increments from the piston 1000? above the gap to 1000? below the gap. The piston at the position 1000? above the gap is referred to as Step 1, and the piston 1000? below the gap is referred to as Step 17.

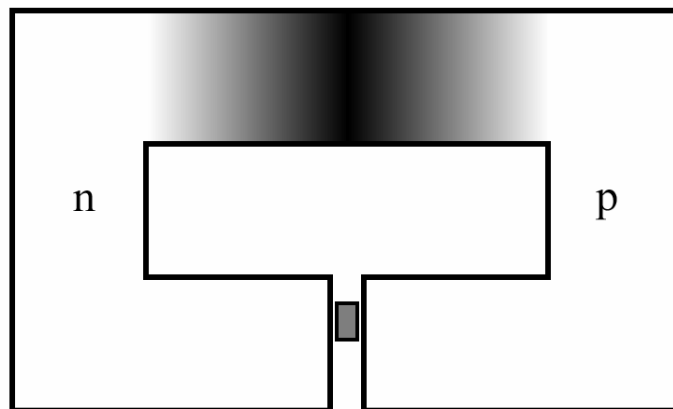


FIGURE 4 – Linear electrostatic motor with slab of intrinsically doped semiconductor in the vacuum gap.

The electrostatic potential energy of the system is shown versus piston position in Figure 5. The figure shows that the majority of the electrostatic potential energy in the system is stored in the n-p bulk, but that there is a sizable energy difference in both the vacuum gap and the n-p bulk between the open gap cases (step 1 and step 17) and the bridged gap cases (step 4 through step 14). The symmetric case in step 9 shows an energy difference of 3×10^{-12} J/m in the overall system energy.

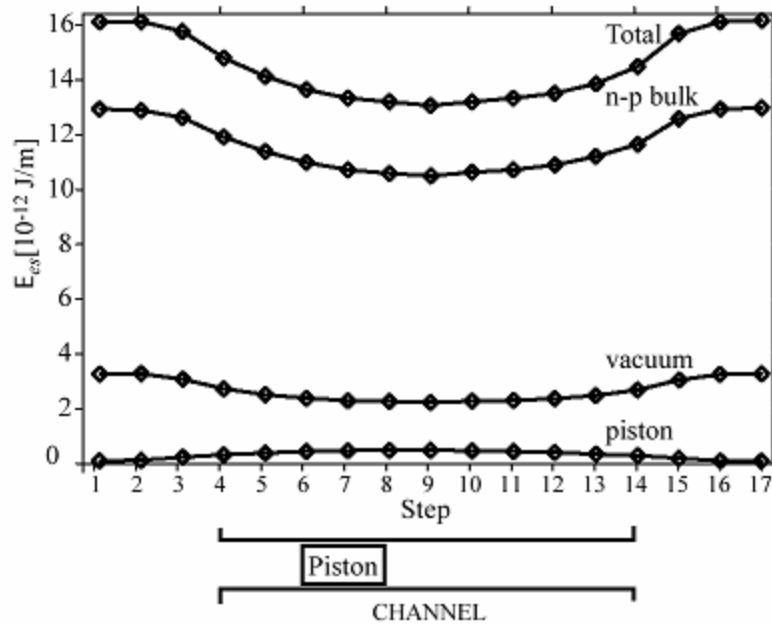


FIGURE 5 – Electrostatic potential energy versus piston position.

Based on the principle of virtual work and the energy minimum at step 9, the piston should be drawn inward toward the piston position at step 9. However, since the simulator only produces equilibrium solutions, it cannot account for the spatially asymmetric energy depression caused by the piston motion. The piston at step 9 could therefore still be subject to a potential gradient. The piston could then move perpetually through the channel [2].

In summary, the 2-D simulations appear to support the 1-D analytical model and shows that, even under the realistic conditions accounted for by the simulator, the device appears plausible.

REFERENCES

1. Sheehan, D. P., Putnam A. R., and Wright, J. H., Found Phys. 32, 1557-1595 (2002)
2. Wright, J. H., QLSL 2002 Proceedings (2002)
3. Silvaco International Corp., ATLAS User's Manual, Silvaco Corp., Santa Clara, CA 2000